Localized Beating between Dynamically Generated Frequencies

G. Kozyreff,[1] M. Tlidi,[1] A. Mussot,[2] E. Louvergneaux,[2] M. Taki,[2] and A. G. Vladimirov[3]

[1]*Optique Nonlinéaire Théorique, Université libre de Bruxelles (U.L.B.), C.P. 231, Campus Plaine, B-1050 Bruxelles, Belgium*

[2]*Laboratoire de Physique des Lasers, Atomes et Molécules, CNRS UMR 8523, Centre d'Etudes et de Recherche Lasers et Applications, Université des Sciences et Technologies de Lille, F-59655 Villeneuve d'Ascq, France*

[3]*Weierstrass Institute for Applied Analysis and Stochastics, Mohrenstrasse 39, D-10117 Berlin, Germany*

(Received 16 May 2008; published 29 January 2009)

We analyze the beating between intrinsic frequencies that are simultaneously generated by a modulation (Turing) instability in a nonlinear extended system. The model studied is that of a coherently driven photonic crystal fiber cavity. Beating in the form of a slow modulation of fast intensity oscillations is found to be stable for a wide range of parameters. We find that such beating can also be localized and contain only a finite number of slow modulations. These structures consist of dips in the amplitude of the fast intensity oscillations, which can either be isolated or regularly spaced. An asymptotic analysis close to the modulation instability threshold allows us to explain this phenomenon as a manifestation of homoclinic snaking for dissipative localized structures.

DOI: 10.1103/PhysRevLett.102.043905 PACS numbers: 42.65.Sf, 42.60.Da, 47.54.−r, 82.40.Bj

One of the most basic and useful experiments in physics is to superimpose two sinusoidal signals with similar frequencies and produce beating—modulation of the mean frequency by an envelope at the difference frequency. An everyday example of this is the moiré pattern produced by folding a sheer window curtain onto itself. This slow modulation can be particularly useful for metrology purposes: in the space domain, moiré allows one to monitor micromechanical deformations [1] while temporal beating can be used to completely characterize ultrashort optical pulses [2]. Usually, the two signals at the origin of beating are generated externally. In this Letter, however, we study numerically and analytically the situation where these emerge spontaneously out of a modulation instability (MI) with threshold. This instability is commonly referred to as Turing instability in chemistry and in biology. The physical setting we have in mind for this study is that of an optical cavity containing a photonic crystal fiber (PCF). In this system, it was shown that two distinct frequencies are generated at the instability threshold [3]. Such a situation is not uncommon in nonlinear optics. Other examples are the double-pass optical loop studied in [4,5], the broad area two-photon resonant Kerr cavity [6], and broad area cavities with nonlocal interactions [7]. Another two-dimensional example is the model proposed in [8] for Faraday waves. In the last three examples, beating is spatial rather than temporal and could therefore involve more than one dimension. We find that, while fast oscillations at the mean frequency do emerge past the MI threshold, the accompanying slow modulation sets in only *locally*; see Fig. 1. In other words, the beating is localized. This phenomenon is robust, stable, and results from the nonlinear saturation that follows the onset of MI. In addition, the number of slow modulations (four in the example of Fig. 1) depends on the initial conditions, which indicates very rich dynamics. We explain this finding through an asymptotic analysis near the MI threshold.

Inside a PCF cavity, the envelope of the electromagnetic field is governed by [3]

$$\frac{\partial \psi}{\partial t'} = S - (1 + i\Delta)\psi + i|\psi|^2\psi - iB_2\frac{\partial^2 \psi}{\partial \tau'^2} + iB_4\frac{\partial^4 \psi}{\partial \tau'^4}. \tag{1}$$

In this equation, the t' dependence corresponds to the slow, average evolution of ψ from one cavity round trip to the next, while τ' corresponds to its fast variations; the parameter S is real and proportional to the injected field, Δ is the cavity detuning, and B_2 and B_4 account for second and fourth order chromatic dispersion, respectively. Finally, $i|\psi|^2\psi$ is the Kerr nonlinearity. The last term in (1) is usually omitted in fiber cavity models [9], but the disper-

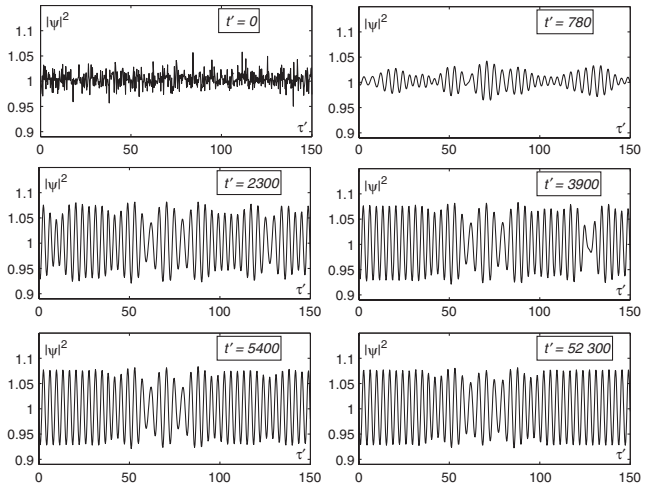

FIG. 1. Snapshots of the numerical integration of (1) for various values of t' with $S = 1.02185$, $\Delta = 0.8$, $B_2 = -1$, $B_4 = 0.2$.

sion characteristics of PCF may invalidate this approximation [10,11], even if B_4 is small. On the other hand, we focus on the situation where third-order dispersion is negligible: this somewhat simplifies the complicated dynamics we are about to describe. Moreover, this can be realized without difficulty with PCF.

We start by assuming that dispersion is anomalous. Thus, the coefficient B_2 is negative and it can be scaled down to -1 by an appropriate choice of unit for τ'. In that case, given the conventional PCF dispersion coefficients $\beta_{2,4}$, group velocity v, and the cavity power loss rate α, one has

$$B_2 = -1, \qquad B_4 = \alpha\beta_4/(12\beta_2^2 v), \tag{2}$$

and we will assume in addition that $B_4 > 0$.

At the MI threshold, the constant solution becomes unstable with respect to perturbations of the form $\exp(i\Omega_U\tau')$ and $\exp(i\Omega_L\tau')$. The two dynamical frequencies are given by

$$\Omega_{L,U}^2 = \frac{1}{2B_4} \pm \frac{\sqrt{1 + 4(\Delta - 2)B_4}}{2B_4}. \tag{3}$$

This formula, incidentally, shows how important B_4 can be despite its smallness.

As a first step to analyze the dynamics, we perform the linear stability analysis of the homogeneous steady state solution of (1). The steady state is given by $\psi = \sqrt{I}\exp(i\phi)$, where

$$S = \sqrt{1 + (\Delta - I)^2}\sqrt{I}, \qquad \tan\phi = I - \Delta, \tag{4}$$

and can thus be parametrized by the intracavity intensity I. The MI threshold is located at $I_{\mathrm{MI}} = 1$. Anticipating a weakly nonlinear analysis near this threshold, and focusing on the "beating limit" $\Omega_U \approx \Omega_L$, we introduce a small parameter ϵ and set

$$I = 1 + 2\epsilon^2\lambda, \qquad \Delta = 2 - 1/(4B_4) + 2\epsilon. \tag{5}$$

The result of the linear stability analysis in that limit is depicted in Fig. 2. In particular, we note that by scaling Δ as above, we get $\Omega_{U,L} \sim \Omega_C \pm \sqrt{\epsilon}$, i.e., a mean frequency $\Omega_C = 1/\sqrt{2B_4}$ and a beat note $2\sqrt{\epsilon}$. The other scalings are standard: the growth rate of unstable perturbations is $O(\epsilon^2)$ and frequency bands of $O(\epsilon)$ width become unstable around Ω_U and Ω_L. These observations suggest to seek a multiple-scale solution of the form

$$\psi \sim e^{i\phi}\left(\sqrt{I} + \sum_n \epsilon^n f_n(t, s, \tau)\right), \tag{6}$$

where

$$t = 2\epsilon^2 t', \qquad s = \Omega_C\tau', \qquad \tau = \sqrt{\epsilon}\tau'.$$

In addition, ϕ should be expanded as $\phi_0 + \epsilon\phi_1 + \cdots$ in order to satisfy (4), given (5).

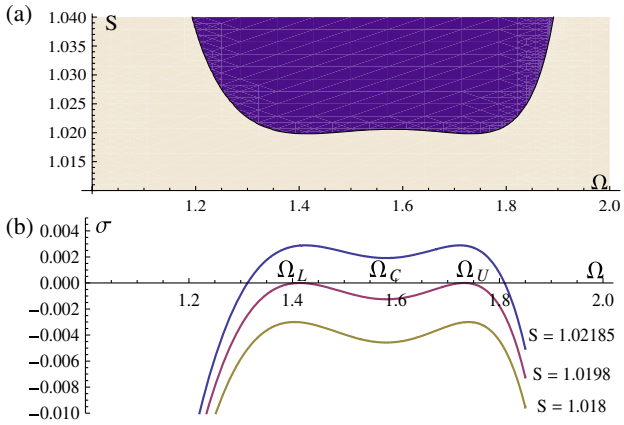

FIG. 2 (color online). Linear stability analysis of the solution (4) for the parameters of Fig. 1. (a) Instability domain in the Ω-S plane. (b) Growth rate σ of perturbations as a function of frequency near MI threshold.

Substituting the asymptotic expansion (6) into (1), we obtain, at $O(\epsilon)$, the linear problem

$$\mathcal{L}f_1 \equiv \left(1 + \frac{\partial}{\partial s^2}\right)^2 f_1 + 4B_4(if_1 + \bar{f}_1) = 0,$$

where the overbar is used to denote complex conjugate. The above equation possesses the nontrivial solution

$$f_1 = \sqrt{i}u(t, \tau)\cos(s), \tag{7}$$

where u is real and to be determined at subsequent orders of the analysis. Note that for any complex function $w(t, \tau)$, one has $\mathcal{L}[w\cos(s)] - i\overline{\mathcal{L}[w\cos(s)]} = 0$. Hence the solvability condition for the equation $\mathcal{L}f = g\cos(s)$ is that $g - i\bar{g}$ vanish. This condition is automatically satisfied for the problem obtained at $O(\epsilon^2)$, and we find at this order that

$$\begin{aligned} f_2 = {} & 2B_4[(-2 - i) + 4(1 + i)B_4]u^2 \\ & + \frac{2B_4}{81}[(-18 - 9i) + 4(1 + i)B_4]u^2\cos(2s) \\ & + \sqrt{2}\left(\frac{\partial^2 u}{\partial\tau} + u\right)\cos(s). \end{aligned}$$

Finally, evaluating the solvability condition at $O(\epsilon^3)$, we obtain

$$\frac{\partial u}{\partial t} = \lambda u - \kappa u^3 - \left(1 + \frac{\partial^2}{\partial\tau^2}\right)^2 u, \tag{8}$$

where $\kappa = 2B_4(171 - 326B_4)/81$.

We have thus shown that the envelope u satisfies the well-known Swift-Hohenberg equation. The derivation of (8) is a considerable progress with respect to (1), as it has already been the subject of numerous studies in the frame of pattern formation. On the other hand, to obtain (8) near the MI threshold is also somewhat surprising because one usually expects a Ginzburg-Landau equation in that limit.

Actually, if Ω_U and Ω_L are well apart, the resulting asymptotic description is a pair of coupled Ginzburg-Landau equations, each governing the amplitude of oscillations at one of the two frequencies. Let us remark that (8) is valid only if its cubic term is saturating, i.e., if $B_4 < B_4^* = 171/326$.

Equation (8) shows that two frequencies become unstable at $\lambda = 0$, in agreement with the MI behavior of (1). An homogeneous solution, corresponding to oscillation at Ω_C, exists for $\lambda = 1$ and is stable for $\lambda > 1.5$. On the other hand, (8) admits localized solutions [12–14], which have been linked to localized structures in optics [15,16], solid mechanics [17,18], and fluid dynamics [19–21]. The bifurcation diagram associated to these solutions generally assumes an infinite series of folds whereby the localized state acquires or loses a pair of peaks, as shown in Fig. 3. A convenient measure of these solutions is the ''energy'' N of their oscillations. One way to define it is

$$N = \sqrt{\kappa} \int_{-\infty}^{\infty} |u - u_\infty| d\tau,$$

where u_∞ is the homogeneous (Ω_C) solution. With such a norm, the folds of the bifurcation diagram generally assemble into two interweaved snaking curves. The phenomenon giving rise to localized solutions is thus often referred to as homoclinic snaking. In most cases, the two aforementioned snaking curves delimit a finite range of parameters where localized states exist—the ''pinning range.'' In the special case of Eq. (8), however, the snakes extend to infinity [22], and so does the existence domain of localized states. Looking back at expression (7), we see that localized solutions of (8) actually describe localized beating solutions in the original model (1), as illustrated schematically in Fig. 4. Consequently, localized beating can be understood as an indirect manifestation of homoclinic snaking. The localized beating is between the frequencies Ω_L and Ω_U and happens over a background oscillating at the central frequency Ω_C.

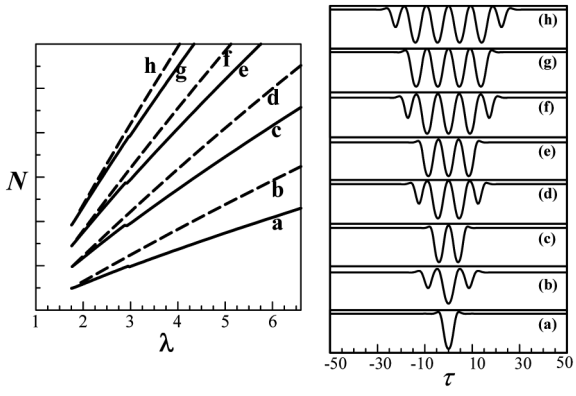

FIG. 3. Left: Bifurcation diagram for the localized structures of (8). Solid lines indicate stable solutions, broken lines indicate unstable solutions. The bifurcation curves extend to arbitrary large and positive values of λ. Right: Representative solutions of the various branches on the left.

It should be emphasized that (8) is only valid for $\epsilon \ll 1$. Hence, given that $I = 1 + \epsilon^2 \lambda$, the range of existence of localized beating solutions is not necessarily large in the full model, even though it is infinite in the Swift-Hohenberg limit. Nevertheless, we found that key features of homoclinic snaking, such as the multiplicity of localized beating solutions, are preserved in the original model. Moreover, in Fig. 3, we see that the minimum value of λ to observe localized beating is given by $\lambda_{\mathrm{LB}} \approx 1.8$. Substituting these values into (5), we obtain a nonlinear threshold for localized beating: $I_{\mathrm{LB}} \approx 1 + 0.9[\Delta - 2 + 1/(4B_4)]^2$. This is a finite distance above the MI threshold. For the parameters of Fig. 1, for instance, we obtain $I_{\mathrm{LB}} = 1.002\,25$, and the corresponding value of the injection parameter is $S_{\mathrm{LB}} = 1.021\,39$. This is in very good agreement with our numerical simulations of (1). In addition, the beating period of 20 in Fig. 1 corresponds to the theoretical beat note equal to 0.32. For these simulations, we used the implicit Euler method with discretization steps $\delta t' = 0.78$ and $\delta\tau' = 0.25$ in the t' and τ' variables, respectively, together with periodic boundary conditions in τ'.

If, instead of the above analysis, we assume that chromatic dispersion is normal, $B_2 = +1$, then MI can still occur but this time with $B_4 < 0$. In that case, only one frequency is found to be destabilized at the MI threshold, making Fig. 2 and hence (8) inappropriate to discuss the dynamics. Nevertheless, we still find localized beating, as shown in Fig. 5. The multiplicity of solutions is strongly reminiscent of homoclinic snaking, although the period of the slow modulation now suggests the dominance of two modes within a single, narrow band of unstable frequencies. This shows that localized beating is a very robust phenomenon and that it exists well outside the asymptotics limits where our analytical results strictly hold.

We now discuss some possible experimental parameter values relevant to the present investigation. The general experimental setup is similar to that of previous experimental investigations of MI in fiber cavities, such as [23,24]. Let us assume a PCF with dispersion coefficients $\beta_2 = -1.45 \times 10^{-29}\ \mathrm{s^2\,m^{-1}}$ and $\beta_4 = 1.15 \times 10^{-55}\ \mathrm{s^4\,m^{-1}}$. At each cavity round trip, a fraction of the electromagnetic power is lost through an output coupler with an amplitude transmission coefficient T. Given the cavity length L, the

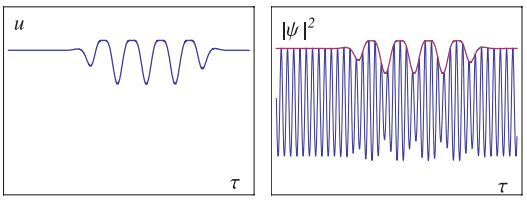

FIG. 4 (color online). Schematic example of a localized solution of the amplitude Eq. (8) and the corresponding localized beating solution of (1), as constructed from (7).

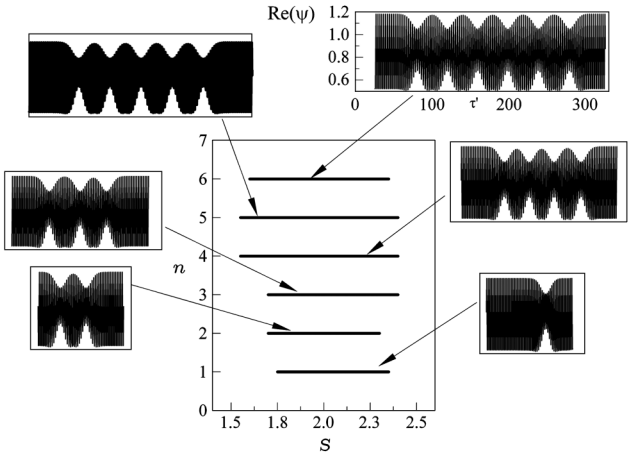

FIG. 5. Numerically determined range of existence of localized beating solutions as a function of S, where n denotes the number of modulations. $\Delta = 1.5$, $B_2 = 1$, $B_4 = -0.25$.

power loss per unit time is therefore $\alpha = T^2 v/L$, and we thus have $\alpha/v = T^2/L$ in (2). With the above PCF characteristics and the typical value $T = 0.35$, a cavity length $L = 27.9$ m yields $B_4 = 0.2$. Interestingly, the critical value $B_4 = B_4^*$ could be reached by reducing the cavity length to $L = 10.64$ m. In this regard, we note that as B_4 approaches and surpasses B_4^*, Eq. (8) should generally be completed by a quintic nonlinearity. This, in turn, is known to result in a finite pinning range [25].

In conclusion, we have revisited the concept of beating for nonlinear extended systems where the source of oscillation is a modulation instability. Through the nonlinearity, the beating can self-organize and become localized in time. By means of a multiple-scale reduction near the instability threshold, we have been able to link this phenomenon with the homoclinic snaking that takes place in the Swift-Hohenberg equation. Moreover, since our analysis is local, this reduction should in principle hold for any system whose linear stability is as depicted in Fig. 2. Such systems have not been particularly sought after in the past, but the present study certainly prompts one to investigate under which physical, chemical, or biological circumstances a modulation instability with two frequencies can arise.

G. K. and M. T. acknowledge financial support from the Fonds National de la Recherche Scientifique (F. R. S.-FNRS, Belgium). A. G. V. acknowledges financial support by the SFB 787 of the DFG. This work was also partially supported by the Interuniversity Attraction Pole program of the Belgian government. The Centre d'Etudes et de Recherches Lasers et Applications is supported by the Ministère chargé de la Recherche, the Région Nord-Pas de Calais and the Fonds Européen de Développement Economique des Régions. We thank S. Métens for bibliographical informations as well as the anonymous referees whose comments significantly improved the manuscript.

[1] *Handbook of Moiré Measurement*, edited by C. A. Walker (Institute of Physics, Bristol, 2003).
[2] P. Kockaert *et al.*, IEEE J. Sel. Top. Quantum Electron. **10**, 206 (2004).
[3] M. Tlidi *et al.*, Opt. Lett. **32**, 662 (2007).
[4] P. Kockaert *et al.*, Opt. Lett. **31**, 495 (2006).
[5] G. Kozyreff *et al.*, Phys. Rev. A **73**, 063815 (2006).
[6] M. Hoyuelos *et al.*, Phys. Rev. E **65**, 046620 (2002).
[7] L. Gelens *et al.*, Phys. Rev. A **75**, 063812 (2007).
[8] R. Lifshitz and D. M. Petrich, Phys. Rev. Lett. **79**, 1261 (1997).
[9] L. A. Lugiato and R. Lefever, Phys. Rev. Lett. **58**, 2209 (1987).
[10] F. Biancalana, D. V. Skryabin, and P. S. J. Russell, Phys. Rev. E **68**, 046603 (2003).
[11] F. Biancalana and D. V. Skryabin, J. Opt. A Pure Appl. Opt. **6**, 301 (2004).
[12] M. Tlidi, P. Mandel, and R. Lefever, Phys. Rev. Lett. **73**, 640 (1994).
[13] G. W. Hunt, G. J. Lord, and A. R. Champneys, Comput. Methods Appl. Mech. Eng. **170**, 239 (1999).
[14] G. Kozyreff and S. J. Chapman, Phys. Rev. Lett. **97**, 044502 (2006).
[15] V. B. Taranenko, I. Ganne, R. J. Kuszelewicz, and C. O. Weiss, Phys. Rev. A **61**, 063818 (2000).
[16] S. Barland *et al.*, Nature (London) **419**, 699 (2002).
[17] G. W. Hunt, M. A. Peletier, A. R. Champneys, P. D. Woods, M. A. Wadee, C. J. Budd, and G. J. Lord, Nonlinear Dynamics **21**, 3 (2000).
[18] M. K. Wadee, C. D. Coman, and A. P. Bassom, Physica (Amsterdam) **163D**, 26 (2002).
[19] H. Sakaguchi and H. Brand, Physica (Amsterdam) **97D**, 274 (1996).
[20] O. Batiste, E. Knobloch, A. Alonso, and I. Mercader, J. Fluid Mech. **560**, 149 (2006).
[21] A. Bergeon and E. Knobloch, Phys. Fluids **20**, 034102 (2008).
[22] J. Burke and E. Knobloch, Phys. Rev. E **73**, 056211 (2006).
[23] S. Coen and M. Haelterman, Phys. Rev. Lett. **79**, 4139 (1997).
[24] M. Stratmann, T. Pagel, and F. Mitschke, Phys. Rev. Lett. **95**, 143902 (2005).
[25] J. Burke and E. Knobloch, Phys. Lett. A **360**, 681 (2007).